Piezomagnetic behavior of Fe-Al-B alloys

Cristina Bormio-Nunes, Olivier Hubert

Piezomagnetic behavior of Fe-Al-B alloys

Cristina BORMIO-NUNES[a,*], Olivier HUBERT[b]

[a] *Escola de Engenharia de Lorena - Universidade de São Paulo - Lorena-SP, Brasil*
[b] *LMT-Cachan (ENS-Cachan / CNRS UMR 8535 / Université Paris Saclay), 61 avenue du président Wilson, 94235 CACHAN Cedex, France*

Abstract

For the first time, the piezomagnetic behavior of polycrystalline Fe-Al-B alloys is accessed. Piezomagnetic factors of up to 4.0 kA.m^{-1}/MPa were reached for an interval of applied compressive stresses between 0 to -140 MPa. The experimental results together with a powerfull multiscale and biphasic modeling allowed the general understanding of the magnetostrictive and piezomagnetic behaviors of these materials. The magnetic and mechanical localizations as well as homogeneous stresses were considered in the modeling and are associated to the intrinsic presence of the Fe_2B phase. The interplay of the magnetocrystalline anisotropy, initial susceptibility, saturation magnetostriction and texture were quantified by the model and compared to the experimental results. An improvement of the piezomagnetic factor to 15 kA.m^{-1}/MPa is predicted, for an alloy containing 20% of aluminum, by getting an adequate texture near $< 100 >$ directions.

Keywords: iron-boron alloys, iron-aluminum alloys, piezomagnetism, magnetostriction, biphasic model, magnetomechanics

*Corresponding author - cristina@demar.eel.usp.br

1. Introduction

For devices that utilize magnetomechanical behavior for their operation, it is necessary to have materials that present large coupling between mechanical and some magnetic properties. Specifically, the variation of the magnetization M with respect to the applied uniaxial stress σ (*i.e.* $dM/d\sigma$) should be high for an appropriate sensitivity [1]. The coupling leads to the thermodynamic condition that $\mu_0.dM/d\sigma = d\lambda/dH$ [2]: λ is the magnetostriction "measured" in the magnetic measurement direction, H is the magnetic field and typical desirable $d\lambda/dH$ values are greater than 1.0 nm/A [1], which is equivalent to 0.83 kA.m^{-1}/MPa for $dM/d\sigma$.

Rare earth elements (Tb, Dy) are often used as secondary elements in alloys that are employed as magnetic sensors or actuators, because they exceptionally enhance the magnetomechanical properties of these materials. For example, Terfenol D presents very high magnetostriction values, typically 1000 ppm at room temperature [3, 4]. The sensitivity of the magnetostriction and magnetization to the application of mechanical stresses, called the magnetomechanical or piezomagnetic behavior is very high for these materials. The variation rate of deformation to the applied field measured at a compression of -9 MPa is 16 nm/A for a bias field of 22 kA/m [4]. Likewise, the sensitivity of the magnetization with respect to the applied stress estimated from the data in [4] is $\sim$ 15 kA.m^{-1}/MPa for an absolute maximum compression value of -25 MPa and 120 kA/m bias field. However, due to the increase of price and limited availability of these rare earth elements, the development of rare earth free alloys is relevant.

Fe-Al alloys demonstrated to be interesting candidates [5]. Fe-Al binary alloys are monophasic for aluminum contents lower than 17% (atomic) and in this range only the α-phase occurs that is a disordered bcc phase with A2 structure. α-phase of pure iron has saturation magnetization of 1.7×10^6 A/m and a anisotropy constant $K_1 = 4.8\times\ 10^4$ J.m^{-3} (cubic symmetry). Both properties decrease monotonically with increasing aluminum content until 17%. In the range $17 <$ % Al < 30 a partial ordering can take place depending on the cooling rate of the material and the ordered Fe_3Al phase with D03 structure can coexist with the α-phase [6, 7]. Fe_3Al phase is also ferromagnetic and has a saturation magnetization of 8.03×10^5 A/m and Curie temperature $T_C = 440$°C [8]. The anisotropy constant K_1 decreases from 2.3×10^4 J.m^{-3} for $\sim$ 17% Al to zero for 22% Al. From 22% Al to 30% Al, $K_1 < 0$ and has a minimum of -0.9×10^4 J.m^{-3} for 26% Al [6]. K_1 is null for 30% of Al [6].

Recently an important increase of the Fe-Al alloys magnetostriction has been observed due to the addition of boron [9]. The introduction of boron to Fe-Al alloys leads to a two or three phases alloy depending on the aluminum content. The boron added to Fe-Al alloys is not soluble in the cubic lattices, but causes the formation of the Fe_2B phase [9]. The as cast microstructure of Fe-Al-B alloys is a dendritic solidified structure in which the dendrites are the Fe-Al cubic phases and the inter-dendritic region is a micro-constituent composed of Fe-Al and Fe_2B phases. A subsequent annealing generates spheroid shaped particles of the Fe_2B phase distributed through the Fe-Al matrix [10].

Fe_2B is also a ferromagnetic phase, which structural, magnetic and magnetostrictive properties are detailed in Appendix A [11, 12]. This material exhibits a positive longitudinal magnetostriction and leads to an enhancement of magnetic and magnetostrictive behavior of the composite formed by Fe-Al matrix and Fe_2B phase.

The influence of boron content has been extensively discussed in a previous work [10]. In the present work, Fe-Al-B were chosen such that the boron atomic fraction was kept constant. The study comprises of four alloys Fe-Al-B alloys, three with fixed B content with composition in the range of $14 < \%\text{Al} < 22$ (at.%) and one sample without aluminum. Magneto-mechanical measurements and microstructure assessment are the tools used to quantify Fe-Al-B alloys piezomagnetic performance. Multiscale modeling considering biphasic material allowed the understanding of the magnetostrictive and piezomagnetic behavior.

2. Expected role of Fe_2B phase in Fe-Al-B ternary alloy

2.1. Composite effect

The influence of the Fe_2B phase inside the Fe-Al matrix can be understood as a composite effect. Indeed the presence of two different phases creates a local perturbation called demagnetizing field in magnetism and residual stress in mechanics [13]. In this condition, the local fields are not generally the same as the mean fields. Their calculation requires a mathematical operation called localization. A medium composed of i phases of volume fraction f_i is considered. The local magnetic field applied to the phase i is a complex function of macroscopic field $\vec{H}$ and the properties of the mean medium. In

the case of spheroidal inclusion [14], the field is demonstrated as homogeneous on each phase. Considering on the other hand a linear susceptibility of average medium χ_m, the local magnetic field in the phase i is given by:

$$\vec{H}_i = \vec{H} + \frac{1}{3+2\chi_m}(\vec{M} - \vec{M}_i) = \vec{H} + \vec{H}_i^d \tag{1}$$

where $\vec{M}$ is the average magnetization, $\vec{M}_i$ is the local magnetization. $\vec{H}_i^d$ is the so called demagnetizing field acting on phase i. The extension to nonlinear behavior involves to use the sequent susceptibility for the definition of χ_m.

$$\chi_m = \|\vec{M}\|/\|\vec{H}\| \tag{2}$$

Averaging operations lead to

$$\vec{H} =< f_i\vec{H}_i > \qquad \text{and} \qquad \vec{M} =< f_i\vec{M}_i > \tag{3}$$

The solution of Eshelby's problem is the basis of the modelling of heterogeneous media's behavior in mechanics. Its formulation has been extended by Hill considering a deformable matrix [15]. Equation 4 gives the stress field within the inclusion i submitted to a macroscopic stress $\boldsymbol{\sigma}$. $\boldsymbol{\epsilon}_i$ is the total strain tensor of the inclusion considered. $\boldsymbol{\epsilon}$ is the average total strain tensor over the volume.

$$\boldsymbol{\sigma}_i = \boldsymbol{\sigma} + \mathbb{C}^\star(\boldsymbol{\epsilon} - \boldsymbol{\epsilon}_i) = \boldsymbol{\sigma} + \boldsymbol{\sigma}_i^r \tag{4}$$

$\mathbb{C}^\star$ is the Hill's constraint tensor depending on the distribution and shape of inclusions and on the stiffness properties of materials. $\boldsymbol{\sigma}_i^r$ is the so called

residual stress tensor acting on inclusion i. If homogeneous isotropic elastic properties (Young's modulus E and Poisson's ratio ν) and additivity of deformation (total deformation = elastic deformation + magnetostrictive deformation) are considered, equation 4 can be simplified in:

$$\boldsymbol{\sigma}_i = \boldsymbol{\sigma} + \frac{E(7-5\nu)}{15(1-\nu^2)}(\boldsymbol{\epsilon}^\mu - \boldsymbol{\epsilon}_i^\mu) \tag{5}$$

where $\boldsymbol{\epsilon}_i^\mu$ and $\boldsymbol{\epsilon}^\mu$ denote the local and average magnetostriction strain tensor respectively.

Averaging operations lead to:

$$\boldsymbol{\sigma} =< f_i\boldsymbol{\sigma}_i > \qquad \text{and} \qquad \boldsymbol{\epsilon}^\mu =< f_i\boldsymbol{\epsilon}_i^\mu > \tag{6}$$

2.2. Application to α phase − Fe_2B phase composite

This approach is applied to α phase − Fe_2B phase microstructure with f_α and f_{Fe_2B} the volume fractions of α phase and Fe_2B phase respectively. The problem is next simplified in a 1D problem (all quantities measured along x axis for example), the average magnetic and magnetization fields verify:

$$H = f_\alpha H_\alpha + f_{Fe_2B} H_{Fe_2B} \tag{7}$$

and

$$M = f_\alpha M_\alpha + f_{Fe_2B} M_{Fe_2B} \tag{8}$$

The average uniaxial stress and longitudinal magnetostriction strain (λ) verify:

$$\sigma = f_\alpha \sigma_\alpha + f_{Fe_2B}\sigma_{Fe_2B} \tag{9}$$

$$\lambda = f_\alpha \lambda_\alpha + f_{Fe_2B} \lambda_{Fe_2B} \tag{10}$$

The magnetic field inside the α phase is given by:

$$H_\alpha = H + \frac{1}{3 + 2\chi_m}(M - M_\alpha) \tag{11}$$

Because Fe_2B phase is very soft (until magnetic rotation out of the easy axis - see Appendix A), $M_{Fe_2B} > M$ so that, due to averaging, $M_\alpha < M$. The magnetic field in the α phase is consequently higher than the average magnetic field (H_α >H), enhancing both magnetization and magnetostriction.

The stress field inside the α phase is given by:

$$\sigma_\alpha = \sigma + \frac{E(7 - 5\nu)}{15(1 - \nu^2)}(\lambda - \lambda_\alpha) \tag{12}$$

Due to soft magnetic properties of Fe_2B phase, longitudinal magnetostriction is higher than average magnetostriction at low magnetization level ($\lambda_{Fe_2B} > \lambda$), so that, due to averaging, $\lambda_\alpha < \lambda$. The stress field in the α phase is consequently higher than the average stress field ($\sigma_\alpha > \sigma$). Considering an unloaded specimen (σ=0), a positive stress is created inside the matrix counterbalanced by a negative stress field in the Fe_2B phase. The longitudinal magnetostriction being positive for α-phase, the positive residual stress leads to enhanced magnetization and magnetostriction properties as well.

This simplified approach allows to explain in few words the composite effect that occurs for Fe-Al-B alloys. It must nevertheless be nuanced be-

cause of the non-linearity of both magnetic and magnetostrictive behaviors, multiaxiality of stress and texture effects (isotropic distribution of phase is assumed). An experimental approach is required to underline these limits.

3. Experimental Methods

The alloys were produced by arc melting in argon atmosphere and re-melted in a high vacuum furnace inside an alumina tube of 25 mm of diameter. The bars obtained had around 110 mm of length and 280 g (figure 1). Plates of thickness of 3 mm were cut from the center in the longitudinal direction of the bars by electro erosion. The plates were annealed in inert atmosphere at 1100°C during 24 h and quenched in water. These plates are the samples studied in this work and had their microstructure and piezomagnetic behavior analyzed.

The microstructure of the samples were characterized by scanning electron microscopy: imaging by secondary electrons, composition by EDX and crystallographic texture by EBSD. The samples preparation for SEM observation consists of mechanical and subsequent electro polishing. The EBSD measurements were made in areas of just about 1.2 mm^2 in both sides of the plates, at the positions where the strain gauges were glued. The anhysteretic piezomagnetic behavior measurement set up acquires the magnetization (M) and longitudinal magnetostriction (λ) under different levels of applied stress varying the magnetic field. For each applied magnetic field, the sample is demagnetized [16]. The active ranges of stresses and magnetic field are -140 $\leq \sigma \leq$ 50 MPa and $0 <$ H $<$ 17 kA/m, respectively.

Figure 1: Typical Fe-Al-B alloy bar of 25 mm in diameter and 110 mm in length

The system consists in a sample plate positioned inside a primary cylindrical coil having 85 turns. Two soft ferrite U-yokes close the magnetic circuit and one strain gauge is glued in each side of the plate to acquire the magnetostriction using also a Wheatstone bridge. To measure the magnetization, a pick up coil of 50 turns is wound in the central region of the plates close to the position of the strain gages. Hydraulic jaws of the tensile-compressive machine used to apply the stress grab the system by the sample. The concentration of boron was determined by atomic absorption in a spectrometer PerkinElmer, model Analyst 800, with an integrated system of graphite furnace and flame. Samples of ~ 0.1 g were analyzed.

4. Experimental results and related modeling

4.1. Microstructure characterization and associated analytical modeling

Figure 2 shows the typical microstructure obtained for the annealed Fe-Al-B alloys. In figure 2 (a) it is possible to verify that the fingerprint of the dendritic solidified microstructure is still present even after the annealing. The Fe_2B lamellas localized in the interdendritic microconstituent (not shown) in the as cast alloys consolidated into a bulk phase as shown in more details in figures 2(b) and (c). The matrix is the Fe-Al binary alloy as discussed previously, but the Fe_2B phase did not form exactly the same spheroid shaped particles as in the previous studies [10]. This may be related to the difference in mass of the samples and thus to different thermal conditions. The mass of the samples in the previous study were 4 g, while it was close to 30 g in the present study.

The measured EDS aluminum content of the matrix of each of the three alloys in atomic percentage and the respective standard deviation are 14.5 $\pm$ 0.2%, 20.2 $\pm$ 0.5% and 22 $\pm$ 0.4%. From now on, we are going to label the samples of these alloys as $A1-14Al$, $A2-20Al$ and $A3-22Al$ and the one without aluminum (x=0) $A0-FeB$. Chemical analyses demonstrate that the mean quantity of boron in the samples is 1.6% and the aluminum contents agree with EDS measurements.

The volume fraction of the phase Fe_2B was evaluated by image analyses and also from EBSD results (associated to low confidence index - CI). The values obtained are very close to 13%. This result is consistent with chemical

183 analyses.

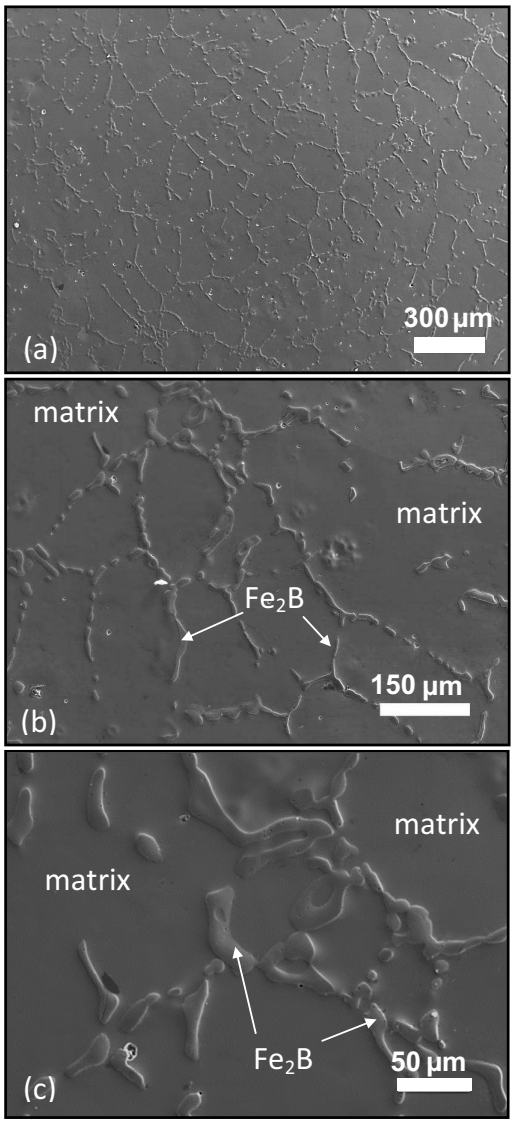

Figure 2: SEM secondary electrons images of the typical microstructure obtained for the Fe-Al-B and Fe-B annealed alloys.

184 Figure 3 shows a typical result obtained from EBSD measurement ($A1-$
185 $14Al$ sample - IPF along X direction), illustrating the large grain size and

186 indexing errors associated to the Fe_2B phase.

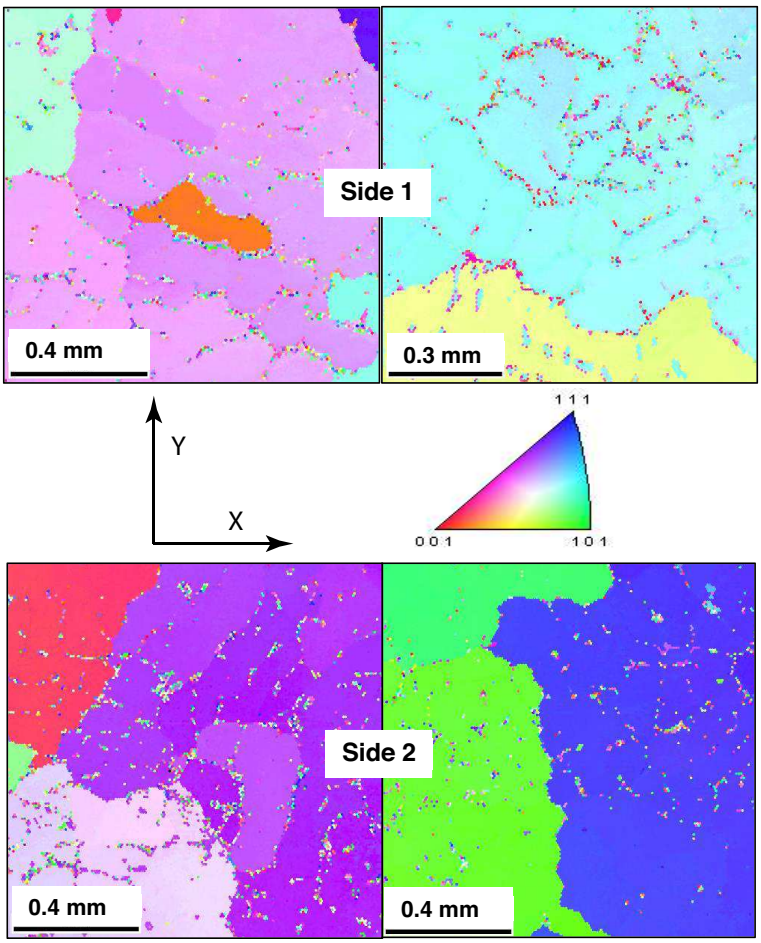

Figure 3: Inverse pole figures (IPF) obtained for the alloy $A1-14Al$ giving the crystallographic direction in the direction of measurement (X). Above are two areas analyzed in one side of the plate and below the other two areas of the other side.

187 EBSD data are composed of Euler angles (ϕ_1, θ, ϕ_2) giving the angular
188 position of a point i (x_i, y_i, z_i) inside the global frame (X, Y, Z) where X
189 indicates the direction of magnetic and mechanical loading. It is possible to
190 calculate the loading direction inside the crystal frame at each EBSD point

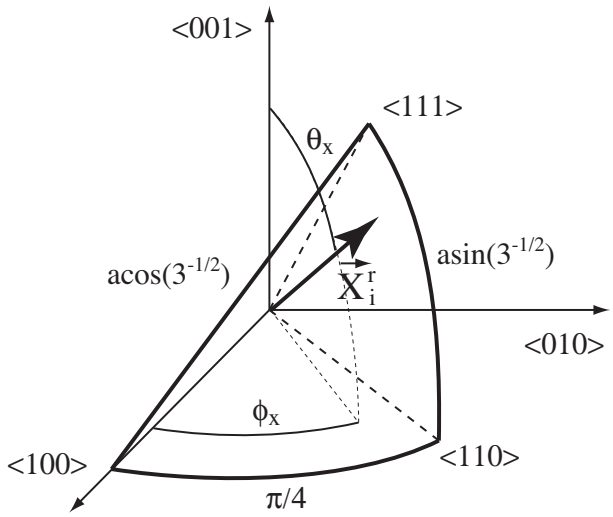

Figure 4: Loading direction $\vec{X}_i^r$ placed inside the standard triangle defined $< 100 >$, $< 110 >$ and $< 111 >$ crystallographic directions after permutation and associated spherical angles.

i (becoming $\vec{X}_i$) of dominant α-phase (Fe_2B phase is not considered). This direction can be expressed inside the standard triangle defined between [100], [110] and [111] crystallographic directions (figure 4) thanks to appropriate permutation operations since the cubic symmetry is considered for the matrix [17]. The corresponding rotated vectors $\vec{X}_i^r$ are averaged over the points i leading to an averaging direction $< \vec{X}^r >$:

$$< \vec{X}^r >= \frac{1}{N} \sum_{i=1}^{N} \vec{X}_i^r \tag{13}$$

The closest associated Miller index $< uvw >$ to $< \vec{X}^r >$ direction is finally estimated. The average orientation results are shown in Table 1 for all samples.

As explained in [18], the behavior of an isotropic polycrystal is necessar-

Table 1: Average orientation of the α phase calculated from EBSD results of Fe-Al-B and Fe-B samples.

Sample	$A0-FeB$	$A1-14Al$	$A2-20Al$	$A3-22Al$
Average orientation	$<421>$	$<321>$	$<420>$	$<421>$

ily given by a loading along a specific direction inside the standard triangle. Because behaviors are not linear, this direction is not the average direction and may change with stress or magnetic field level. Nevertheless it is possible, as first approximation, to consider that an isotropic behavior is roughly obtained when the loading is corresponding to the average direction of the standard triangle. In case of cubic symmetry, this direction is defined by spherical angles $(\phi_X, \theta_X) = (38.81°,\ 77.54°)$, that is close to $<431>$ direction. Samples $A0-FeB$, $A1-14Al$ and $A3-22Al$ may exhibit some barely isotropic behavior since their orientations are close to $<431>$. Sample $A2-20Al$ should exhibit on the contrary a dominant effect of $<100>$ direction.

A theoretical estimation of the magnetostriction without application of external stresses and using the average orientation results is possible after several approximations. Assumptions concern equiprobable initial distribution of domains, homogeneous magnetic and stress fields within the sample. The approach to saturation is on the other hand considered as only depending on anisotropy strength of the material. Indeed α phase could present a low magnetocrystalline constant K_1 that would lead to concomitant rotation

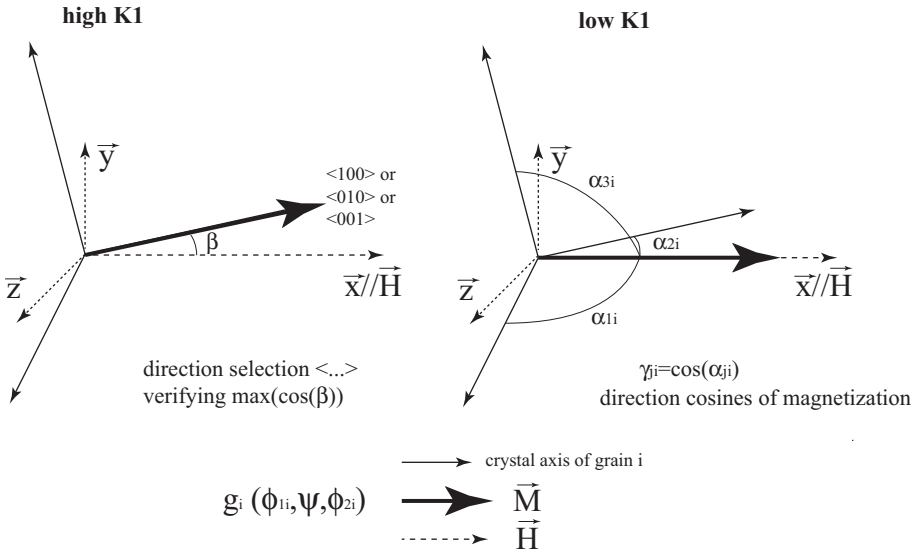

Figure 5: Possible positions of magnetization vector at a position i for high and low magnetocrystalline constant strengths.

and domain wall motion. For high K_1 values, the domain wall motion occurs before rotation and actually in the present case the rotation is supposed to be unachieved.

Figure 5 shows the two possible positions of magnetization vector at a given EBSD point i belonging to the α-phase matrix. These two situations correspond to two different magnetization states under applied field associated with two possible magnetocrystalline constant strengths.

For both situations, two estimations of average longitudinal magnetostriction strain λ are made: $\lambda = \lambda_s$ the saturation magnetostriction if K_1 is "low"; $\lambda = \lambda_{max}$ the maximal magnetostriction if K_1 is high. Each EBSD position i is defined by its Euler angles $(\phi_1^i, \theta^i, \phi_2^i)$ in the macroscopic frame (X, Y, Z)

as shown in figure 5. The magnetic field is applied along X axis. At saturation or considering a low K_1 situation, the magnetization at high field is considered to be aligned with the magnetic field direction. Direction cosines of the magnetization can be deduced because the direction X is known. For a "high" K_1 situation, the magnetic field is supposed not strong enough so that the magnetization direction remains in the direction of one of the three easy axes of the cubic symmetry. The selected direction is obtained by minimizing the angle β, which gives the closest direction to the applied field direction X. In both cases, magnetostriction tensor is calculated at each position i. Equations (14) and (15) give this tensor for low and high K_1 values, respectively.

$$\boldsymbol{\epsilon}_{\mu}^{i} = \frac{3}{2}\begin{pmatrix} \lambda_{100}^{\alpha}(\gamma_1^2 - \frac{1}{3}) & \lambda_{111}^{\alpha}\gamma_1\gamma_2 & \lambda_{111}^{\alpha}\gamma_1\gamma_3 \\ \lambda_{111}^{\alpha}\gamma_1\gamma_2 & \lambda_{100}^{\alpha}(\gamma_2^2 - \frac{1}{3}) & \lambda_{111}^{\alpha}\gamma_2\gamma_3 \\ \lambda_{111}^{\alpha}\gamma_1\gamma_3 & \lambda_{111}^{\alpha}\gamma_2\gamma_3 & \lambda_{100}^{\alpha}(\gamma_3^2 - \frac{1}{3}) \end{pmatrix} \tag{14}$$

$$\boldsymbol{\epsilon}_{\mu}^{i} = \begin{pmatrix} \lambda_{100}^{\alpha} & 0 & 0 \\ 0 & -\frac{\lambda_{100}^{\alpha}}{2} & 0 \\ 0 & 0 & -\frac{\lambda_{100}^{\alpha}}{2} \end{pmatrix} \tag{15}$$

λ_{100}^{α} and λ_{111}^{α} are the independent magnetostriction constants of the α phase cubic single crystal in the directions $< 100 >$ and $< 111 >$. γ_j for j =1, 2 and 3 are the direction cosines of the magnetization as illustrated in figure 5.

As discussed in Appendix A Fe_2B phase exhibits an easy magnetization plane that leads in a first approximation to an enhancement of both magnetic and magnetostrictive properties. This effect is isotropic since the distribu-

tion of Fe_2B phase is considered as isotropic. The averaging operations are made in the framework of homogeneous stress hypothesis: over the EBSD measurement points i first, then considering Fe_2B phase of volume fraction f, as indicated in equations (16) and (17).

$$\boldsymbol{\epsilon}_{\mu}^{\alpha} =< \boldsymbol{\epsilon}_{\mu}^{i} > \tag{16}$$

$$\boldsymbol{\epsilon}_{\mu} = f\boldsymbol{\epsilon}_{\mu}^{Fe_2B} + (1-f)\boldsymbol{\epsilon}_{\mu}^{\alpha} \tag{17}$$

The isotropic distribution of Fe_2B with high intensity uniaxial anisotropy implies that (see Appendix A for detailed calculations) :

$$\boldsymbol{\epsilon}_{\mu}^{Fe_2B} = \frac{1}{2}\begin{pmatrix} \lambda_{100}^{Fe_2B} & 0 & 0 \\ 0 & -\frac{\lambda_{100}^{Fe_2B}}{2} & 0 \\ 0 & 0 & -\frac{\lambda_{100}^{Fe_2B}}{2} \end{pmatrix} \tag{18}$$

leading to the final expression of average magnetostriction strain tensor $\boldsymbol{\epsilon}_{\mu}$. Therefore, an estimation of average magnetostriction strain $\boldsymbol{\epsilon}_{\mu}$ is obtained by using the expression of $\boldsymbol{\epsilon}_{\mu}^{i}$ from equation (14) in the definition of $\boldsymbol{\epsilon}_{\mu}^{\alpha}$ for low K_1. For high K_1 the expression of $\boldsymbol{\epsilon}_{\mu}^{i}$ from equation (15) is used. The magnetostriction strain measured in the direction of applied field is finally given by:

$$\lambda = f\frac{\lambda_{100}^{Fe_2B}}{2} + (1-f)^t\vec{X}\boldsymbol{\epsilon}_{\mu}^{\alpha}\vec{X} \tag{19}$$

Some hypotheses were made concerning the crystallographic ordering of the Fe-Al matrix. The A2 structure (disordered α phase) is chosen as the matrix of samples $A1-14Al$ and $A2-20Al$. For the matrix of sample $A3-$

263 $22Al$, a mix of A2 and D03 structures (ordered phase) with the proportion
264 1:1 is chosen. The physical constants of Fe_2B phase are $\lambda_{100}^{Fe_2B}$= 20 ppm [9].
265 The volume fraction of Fe_2B already previously presented is $f = 0.13$. Table
266 2 shows the values of the Fe-Al matrix physical constants (λ_{100}^{α},λ_{111}^{α}, K_1 [6]),
267 as well as the theoretical and experimental values of the magnetostriction
268 measured in the direction of the applied magnetic field.

Table 2: Physical constants of the Fe-Al matrix [6] complemented by theoretical and experimental parallel magnetostriction measured in the direction of the applied magnetic field (shown in the last two columns).

Sample \ Param.	Structure	λ_{100}^{α}	λ_{111}^{α}	K_1	$\lambda^{calc.}$	$\lambda^{exp.}$
Unit	-	ppm	ppm	kJ.m^{-3}	ppm	ppm
$A0 - FeB$	A2	21	-21	48 (high)	8.6	5.8
$A1 - 14Al$	A2	80	-3	31.3 (high)	21.8	17.3
$A2 - 20Al$	A2	79	4	15.5 (high)	32	25
$A3 - 22Al$	A2/DO3	76/84	7/26	11.5/0 (high/low)	33.5	34.2

269 A relatively good agreement is obtained between theoretical and exper-
270 imental magnetostriction, meaning that orientations are representative of
271 samples. We suppose that except considering a $< 100 >$ oriented sample,
272 the Fe-Al-B alloys of the present work are not good candidate for actuation.
273 The piezomagnetic behavior (magnetization *vs* stress) may be more interest-
274 ing since the performance of such application would depend not only on the
275 magnetostriction magnitude but also on the sensitivity of magnetostriction

to magnetic field ($d\lambda/dH$).

4.2. Magnetic and piezomagnetic behavior

Figure 6 shows the measured curves M *vs.* H for fixed values of stress σ for the four samples. The stress magnitude used for $A0-FeB$ sample is lower than for others samples due to its much lower yield stress. As expected, the magnetization of the sample $A3-22Al$ is smaller than $A2-20Al$ that is smaller than $A1-14Al$ and finally to $A0-FeB$, due to the increase of aluminum content, a nonmagnetic element. It must be noticed that the occurrence of the Fe_3Al (D03) phase would cooperate also to decrease the saturation magnetization in sample $A3-22Al$ [19].

The values of the initial susceptibility are about 1500, 800, 600 and 500 for the correspondingly samples $A0-FeB$, $A1-14Al$, $A2-20Al$ and $A3-22Al$. This trend seems in contradiction with the decreasing of magnetocrystalline constant K_1 with increasing aluminum content. It is on the contrary in accordance with a lower mobility of domain wall due to an increased pinning effect. Indeed magnetostriction is strongly enhanced with aluminum content that increases the magnetoelastic interactions (NB: the reduction of magnetostriction is a well known technique employed to increase the permeability of materials - such for permalloys - [20]).

The M *vs.* σ curves at constant H for each alloy were built from the data of figure 6 for six fixed values of magnetic field in the range of 1-15 kA.m^{-1} and are depicted in figure 7. Subsequently, from these M *vs.* σ curves the respective sensitivity $dM/d\sigma|_H$ is calculated and figure 8 displays the associated plots for each sample at the same values of fixed applied field.

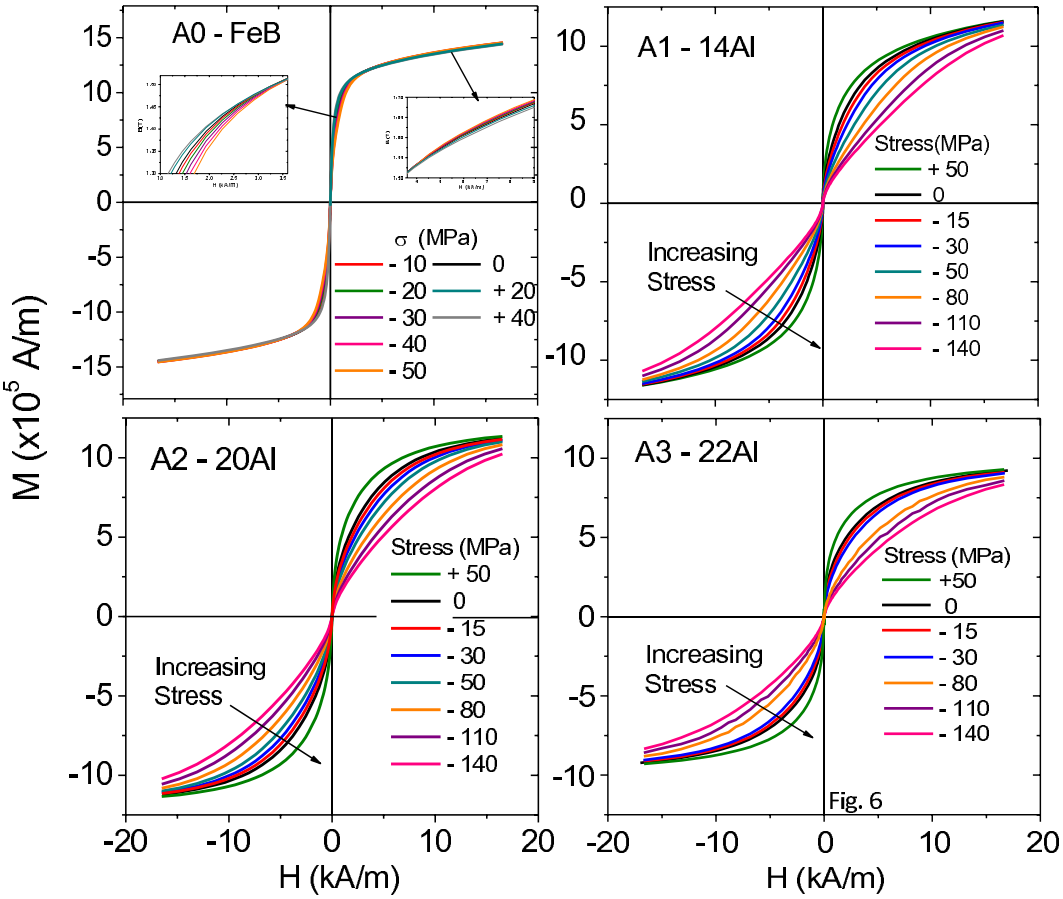

Figure 6: Magnetization as a function of the applied magnetic field for fixed values of stresses for all samples.

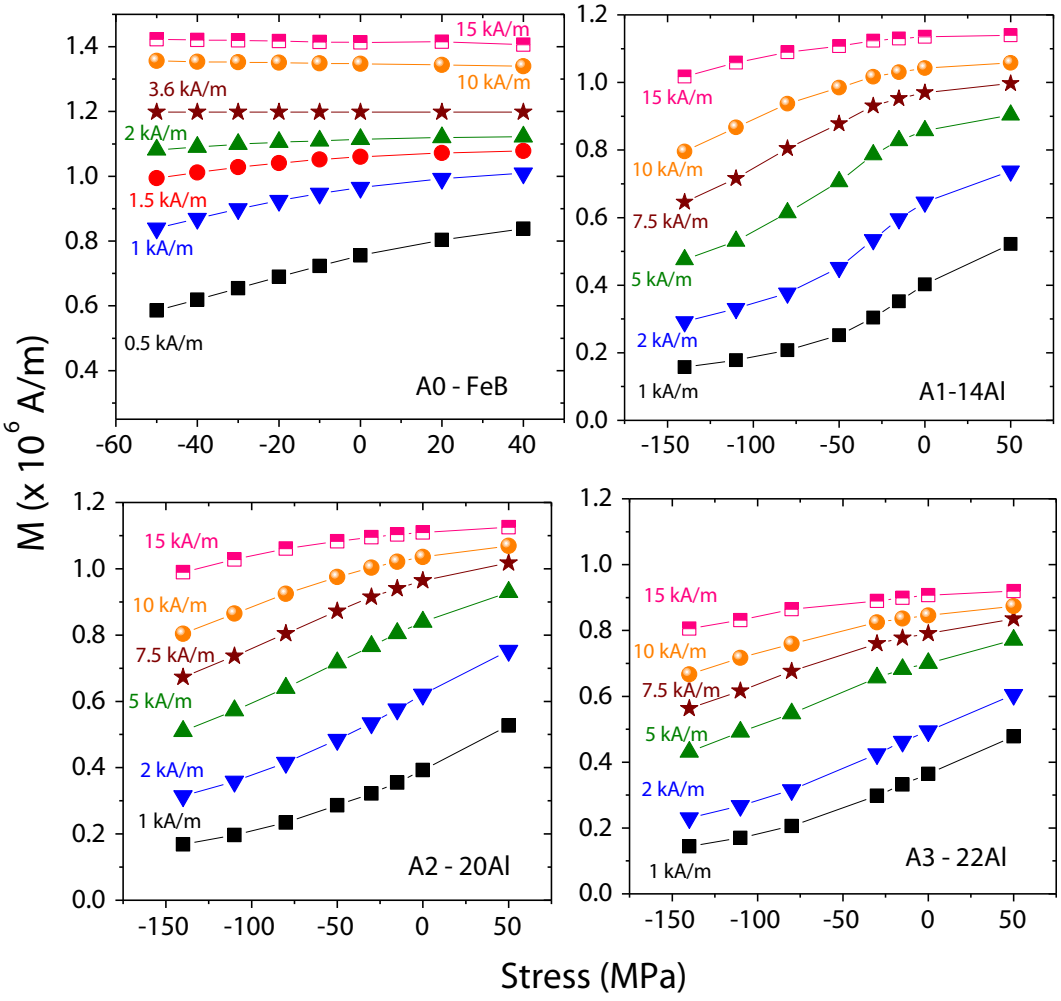

Figure 7: Magnetization as a function of applied stress σ for all samples at fixed values of magnetic field, ($1 \leq H \leq 15$ kA/m).

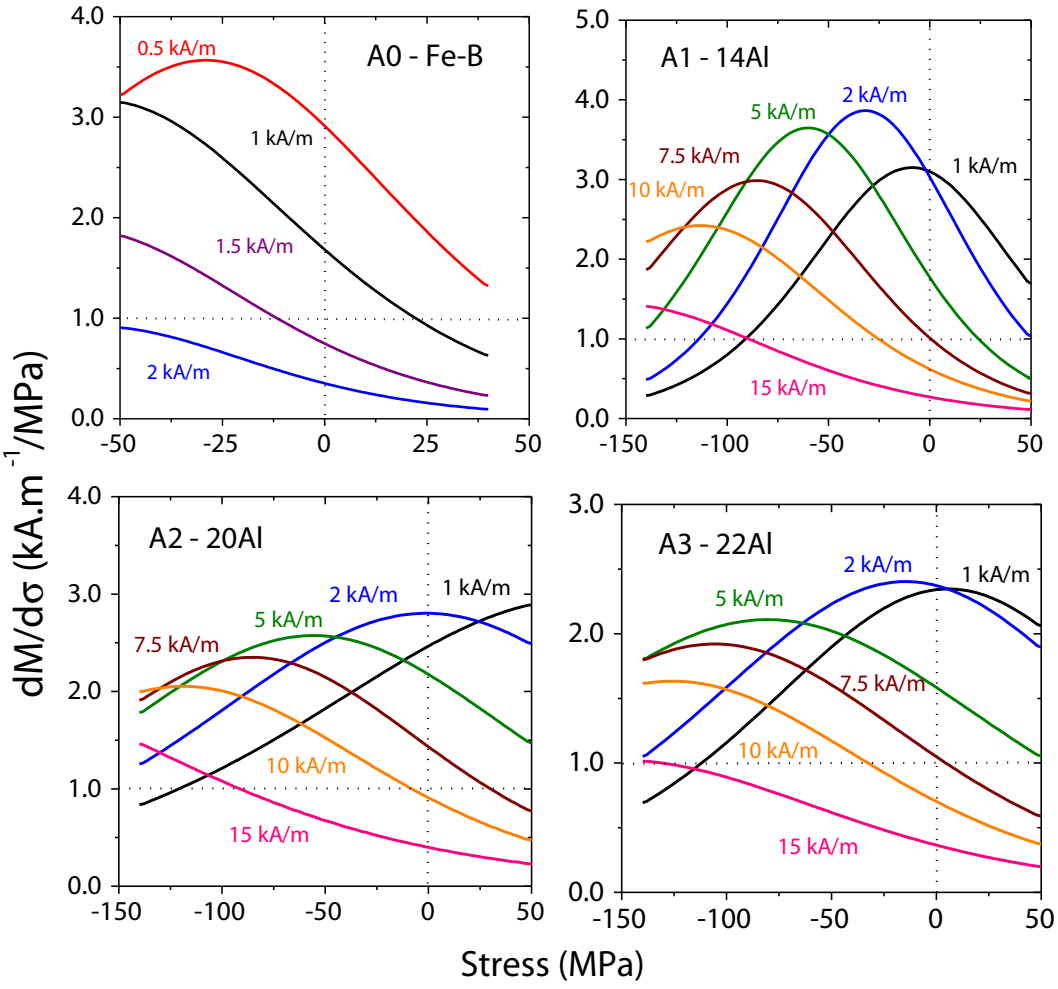

Figure 8: Piezomagnetic sensitivity $dM/d\sigma|_H$ *vs.* σ for all samples at fixed values of magnetic field, ($1 \leq H \leq 15$ kA/m).

By covering all the compression range from 0 to -140 MPa and with sensitivity greater than 1.0 kA.m^{-1}/MPa, there are some different possibilities for using the Fe-Al-B alloys as force sensors. Two of them are described next. For a compression sensor that should work in constant bias field, for all the three alloys, the best bias field is 5.0 kA.m^{-1}. Among them, sample $A2-20Al$ exhibits the largest sensitivity for the entire compression range, between 1.8 and 2.6 kA.m^{-1}/MPa, for a magnetization variation range of about 330 kA.m^{-1}. Although sample $A1-14Al$ has a maximum sensitivity at -30 MPa, *i.e.* 3.9 kA.m^{-1}/MPa. Its sensitivity decreases to 0.5 kA.m^{-1}/MPa at -140 MPa.

A dispositive constructed for varying bias field would employ the interval of $2.0 \leq \mathrm{H} \leq 10$ kA.m^{-1} and in this case, the best alloy would be $A1-14Al$, with sensitivity in the range of 2.2 to 3.9 kA.m^{-1}/MPa for a magnetization variation range of about 710 kA.m^{-1}. Although Terfenol-D has a very high sensitivity of ~ 15 kA.m^{-1}/MPa [4], this material application is restricted to a maximum compression of -25 MPa due to its brittleness. In addition, the bias field is close to 120 kA.m^{-1} that is one order of magnitude higher than the optimal bias field obtained for Fe-Al-B alloys.

Results are interesting and some applicability can arise. It is nevertheless not fully understood why alloy $A1-14Al$ exhibits a higher piezomagnetic sensitivity peak than $A2-20Al$ or $A3-22Al$ although its magnetostriction level is the lowest. Many parameters like saturation magnetization level, anisotropy constant, magnetostriction constants, crystallographic texture, and interaction between matrix and Fe_2B phase must be considered. On the other hand, an increasing of piezomagnetic behavior may be surely reached by a better

choice of crystallographic texture for example. A modeling involving these parameters is presented hereafter.

4.3. Multidomain modeling

A two-scale reversible modeling of the magneto-mechanical behavior of each phase is proposed mixing the propositions of [18] and [21]. This model comes from a simplification of the so-called multiscale model [14] where only domain and grain scales are considered. Even if cubic symmetry is considered, easy directions are not defined *a priori* allowing a statistical description of domain distribution (N domains are considered) and avoiding energy minimization. At each domain ϕ of direction $\vec{\gamma}_\phi = \gamma_i \vec{e}_i$ corresponds a magnetization vector $\vec{M}_\phi = M_s \, \vec{\gamma}_\phi$, and a magnetostriction tensor $\boldsymbol{\epsilon}^\mu_\phi$ (previously defined by equation (14)). This single crystal is considered as submitted to a magnetic field H and/or uniaxial stress σ applied in direction $\vec{X}$ (see table 1) defined by angles ϕ_X and θ_X of the spherical frame (figure 4). It is considered that the contribution to the free energy of a magnetic domain W_ϕ are the magnetostatic energy W^H_ϕ, the magnetocrystalline energy W^K_ϕ and the magnetoelastic energy W^σ_ϕ (20).

$$W^H_\phi = -\mu_0 \vec{H}.\vec{M}_\phi \qquad W^\sigma_\phi = -\boldsymbol{\sigma} : \boldsymbol{\epsilon}^\mu_\phi \qquad W^K_\phi = K_1((\gamma_1\gamma_2)^2+(\gamma_2\gamma_3)^2+(\gamma_1\gamma_3)^2) \tag{20}$$

The volume fraction f_ϕ of a domain is calculated as function of the free energies using the statistical Boltzmann formula (21):

$$f_\phi = \frac{\exp\left(-A_s.W_\phi\right)}{\displaystyle\int_\phi \exp\left(-A_s.W_\phi\right) d\phi} \tag{21}$$

A_s is a parameter related to the initial susceptibility χ_0 of the magnetization curve:

$$A_s = \frac{3\chi_0}{\mu_0 M_s^2} \tag{22}$$

By employing f_ϕ it is possible to calculate the average magnetization $M(H,\sigma)$ and magnetostriction $\lambda(H,\sigma)$ in the direction of applied field/stress by using equations (14) and (23).

$$\vec{M} = \frac{1}{N}\int_\phi f_\phi\, \vec{M}_\phi\, d\phi \qquad \boldsymbol{\epsilon}^\mu = \frac{1}{N}\int_\phi f_\phi \boldsymbol{\epsilon}^\mu_\phi\, d\phi \qquad M = \vec{M}.\vec{X} \qquad \lambda_{//} = {}^t\vec{X}.\boldsymbol{\epsilon}^\mu.\vec{X}. \tag{23}$$

Moreover the following conditions have been used for calculations:

- The possible directions $\vec{\gamma}_\phi$ are described through the mesh of a unit radius sphere. A N=34635 points mesh has been used in the present study.

- Both materials are modeled. Self consistent localization rules are given in section 2.1. Final results are given in term of average behavior. Effect of localization is quickly addressed hereafter.

- EBSD did not allow the measurement of Fe_2B phase orientations. An isotropic distribution of this second phase has been assumed. Uniaxial anisotropy condition allows to consider this phase, in the magnetic field range tested in this study, as a soft isotropic crystal (K_1=0), exhibiting

a saturation magnetization of $M_s^{'Fe_2B} = \frac{\pi}{4} M_s^{Fe_2B}$, a saturation magnetostriction $\lambda_s^{'Fe_2B} = \frac{1}{2}\lambda_s^{Fe_2B}$ and a magnetic susceptibility $\chi_0^{Fe_2B} = 8000$ (see Appendix A for detailed calculations).

- The material parameters used for the modeling of α phase strongly depend on aluminum content. K_1, λ_{100}^{α}, λ_{111}^{α} have already been defined. The aluminum content allows a direct and theoretical estimation of M_s ($M_s^{\alpha}=(1 - at\%Al/100)M_s^{Fe}$). A mix (1:1) of A2 and DO3 structures has been considered for sample $A3 - 22Al$ α phase (mixture rule of all physical constants including saturation magnetization).These parameters are complemented by initial susceptibility χ_0^{α} which has been estimated for each phase independently to fit properly the experimental magnetization measurements. Table 3 gathers the various physical constants used in the modeling.

- The magnetic parameters are complemented by Young's modulus and Poisson's ratio mechanical parameters used to express the mechanical localization. Young's modulus and Poisson's ratio of pure iron have been chosen (see Table 3).

- As already underlined, direction $\vec{X}$ can be restricted to the standard triangle due to cubic symmetry. The average crystallographic direction is considered first (see table 1). Figure 9 shows the magnetostrictive behavior predicted by the model along the longitudinal direction when this direction is considered. A discrepancy is clearly observed between saturation values from experiments (table 2 - figure 10a) and model. This discrepancy can be explained by the fact the average behavior

is not obtained along the average direction. The loading direction has consequently been optimized in regards to magnetostriction experimental values. Table 4 gathers the old and new spherical angles used in the modeling of all samples. This optimization leads to small angle variations (except for sample $A2-20Al$) or no angle variation (sample $A3-22Al$), enough to improve the modeling results of magnetostrictive behavior as illustrated in figure 9 to be compared to figure 10. This direction is kept constant for all loading levels.

Table 3: Parameters used in the modeling of α and Fe_2B phases.

Phase \ Param.	K_1	λ_{100}	λ_{111}	M_s	χ_0	E	ν
Units	$kJ.m^{-3}$	ppm	ppm	$10^5 A.m^{-1}$	-	GPa	-
α - $A0-FeB$	48	21	-21	17.1	1000	200	0.3
α - $A1-14Al$	35.5	80	-3	14.7	700	200	0.3
α - $A2-20Al$	15.5	79	4	13.7	500	200	0.3
α - $A3-22Al$	5.25	80	16.5	10.7	400	200	0.3
Fe_2B	0	10	10	9.4	8000	200	0.3

4.4. Modeling results

Influence of aluminum content

Figures 11 to 13 show the result of modeling for magnetization curves under stress, magnetization *vs* stress at different magnetic field levels (same set of values than for experiments), and piezomagnetic sensitivity *vs* stress at the same magnetic field levels. It can be observed that the model reproduces

Table 4: Spherical angles (°) corresponding to loading direction $\vec{X}$: average directions (corresponding to Miller index reported in table 1) compared to optimized directions.

Sample	ϕ_X av.	θ_X av.	ϕ_X opt.	θ_X opt.
$A0 - FeB$	28	77	31	75
$A1 - 14Al$	36	73	38	70
$A2 - 20Al$	23	82	34	76
$A3 - 22Al$	28	76	28	76

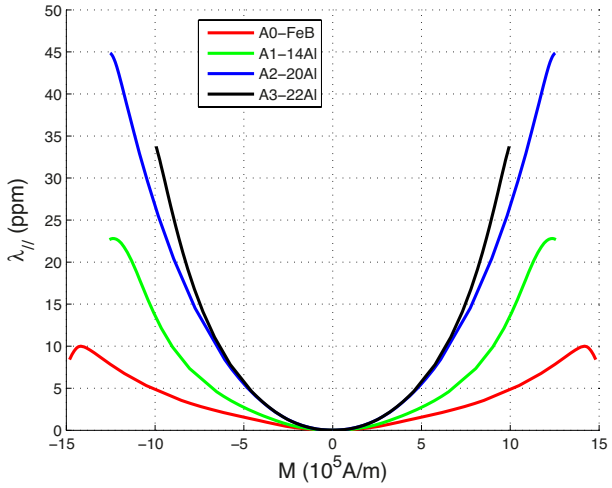

Figure 9: Initial modeling of magnetostriction in the direction of applied field.

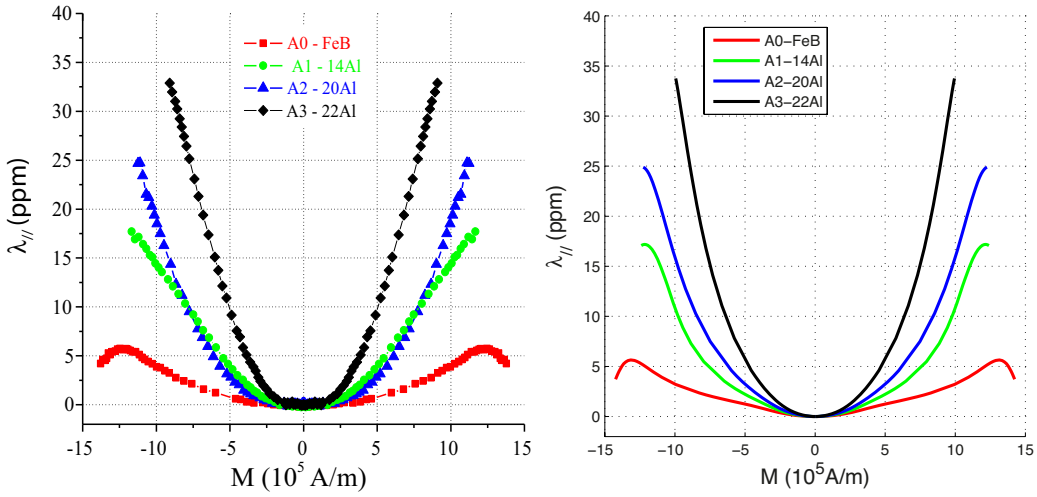

(a) (b)

Figure 10: (a) Experimental measurement of the longitudinal magnetostriction of samples $A0$ to $A3$; (b) new modeling of magnetostriction after optimization of applied field direction taking account of behaviors non-linearity.

accurately all behaviors. Experimental and modeled values of piezomagnetic sensitivity are in accordance. The stress and magnetic levels where maximum piezomagnetic sensitivity is reached are in accordance too. It is nevertheless observed that $A2-20Al$ and $A3-22Al$ samples lead to the highest sensitivity in contradiction with experiments where the maximum sensitivity was reached for $A1-14Al$ sample. Such result could be improved by a better choice of initial susceptibility values for phases. Indeed due to a miss of experimental data the initial susceptibility of Fe_2B phase remains unknown, like initial susceptibility of α phase for all samples. This choice is crucial since initial susceptibility enter in the expression of A_s parameter that defines the sensitivity to field and to stress through their energy expression. Moreover the calculated values of samples $A0$ and $A1$ that exhibit a A2 α

phase are much closer to experimental results than samples $A2$ and $A3$. It seems clear that due to uncertainty on ordered Fe_3Al phase quantity and to its influence on domain wall mobility, initial susceptibility of alloys $A2$ and $A3$ matrix is not a confident parameter.

Effect of Fe_2B phase

Figure 14 illustrates the modeled magnetic and magnetostrictive behaviors of both phases and average medium for $A1-14Al$ sample. This figure illustrates the localization phenomenon. Due to the high initial susceptibility of Fe_2B phase, the composite initial susceptibility is higher than the susceptibility of the pure α phase. On the contrary, the high uniaxial anisotropy and low saturation magnetization of Fe_2B phase lead to a global decrease of magnetic performances of the composite at magnetic field higher than 2 kA/m comparing to pure α-phase. Due to the low magnitude of Fe_2B phase magnetostriction, the magnetostriction magnitude of the composite is usually lower than the magnetostriction magnitude of pure α phase. This point seems in contradiction with results obtained in [9] and [10]. The variations that have been observed were probably related to variations in the samples texture.

Figure 15a and 15b allow the comparison of modeled piezomagnetic sensitivity of $A1-14Al$ α phase only, $A1-14Al$ sample considering localization, and $A1-14Al$ sample considering homogeneous stress and field for two different magnetic field levels (1 kA/m and 2 kA/m). These figures show on the one hand that localization always improve the sensitivity comparing to the homogeneous fields condition. This enhancement effect due to localization

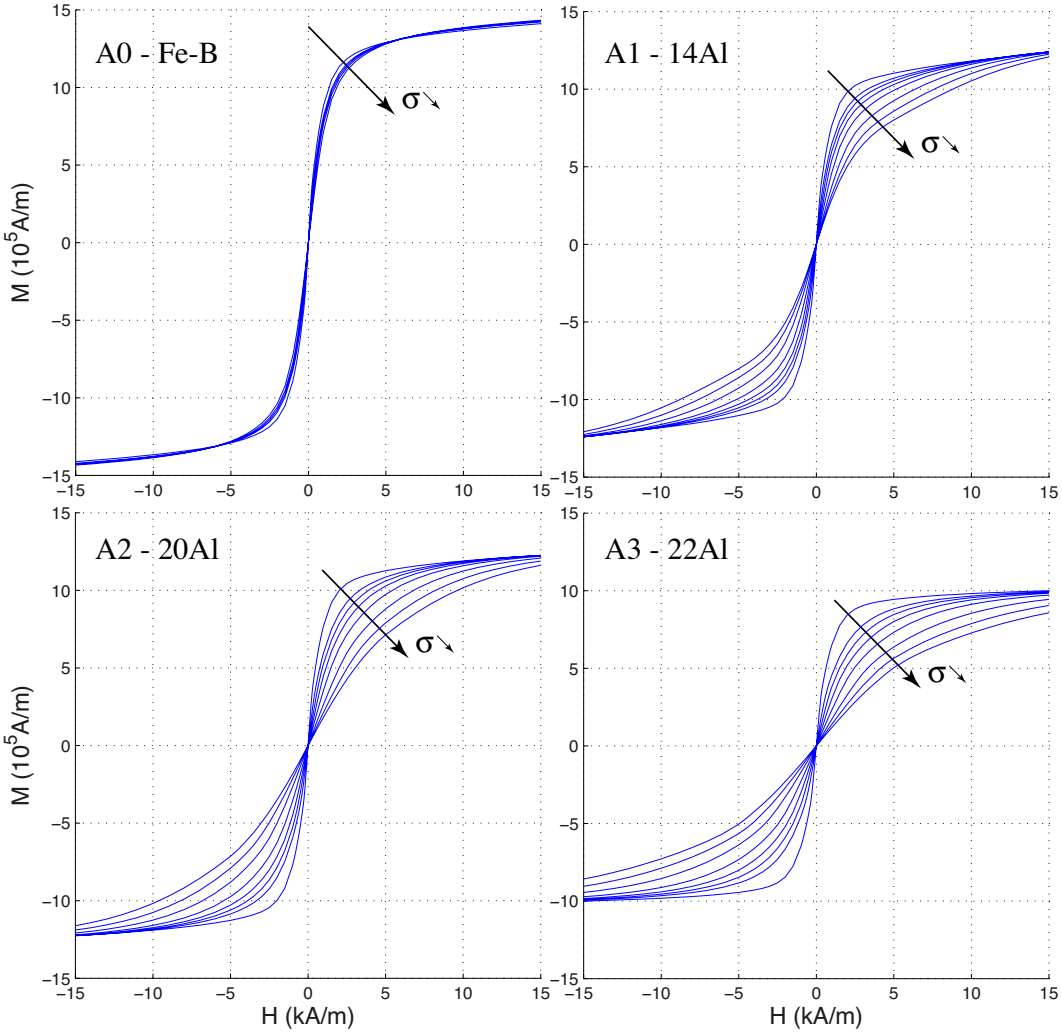

Figure 11: Modeling results: magnetization as a function of the applied magnetic field for fixed values of stresses for all samples ($\sigma \in [50, 0, -15, -30, -50]$ MPa for $A0 - FeB$ sample; $\sigma \in [50, 0, -15, -30, -50, -80, -110, -140]$ MPa for $A1$ to $A3$ samples).

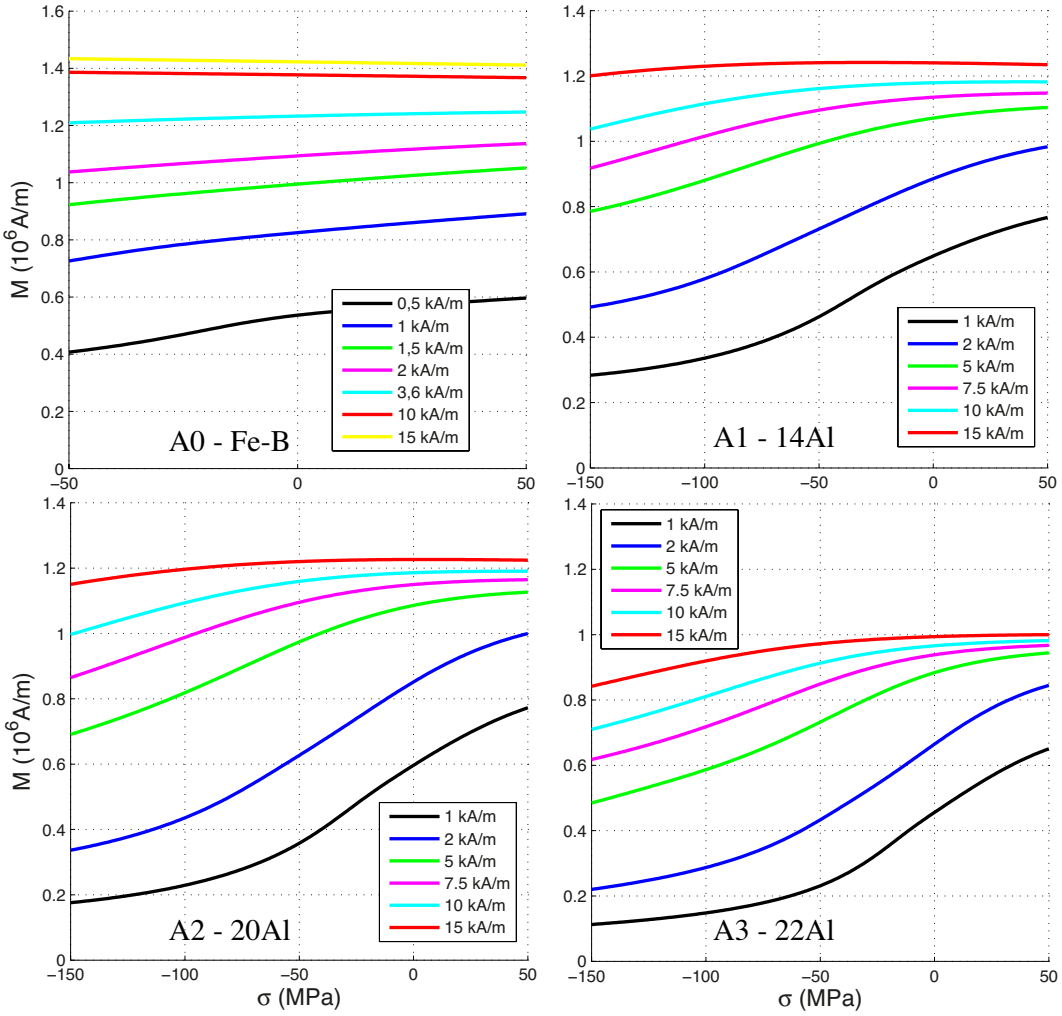

Figure 12: Modeling results: magnetization as a function of applied stress σ for the all samples at fixed values of magnetic field, ($1 \leq H \leq 15$ kA/m).

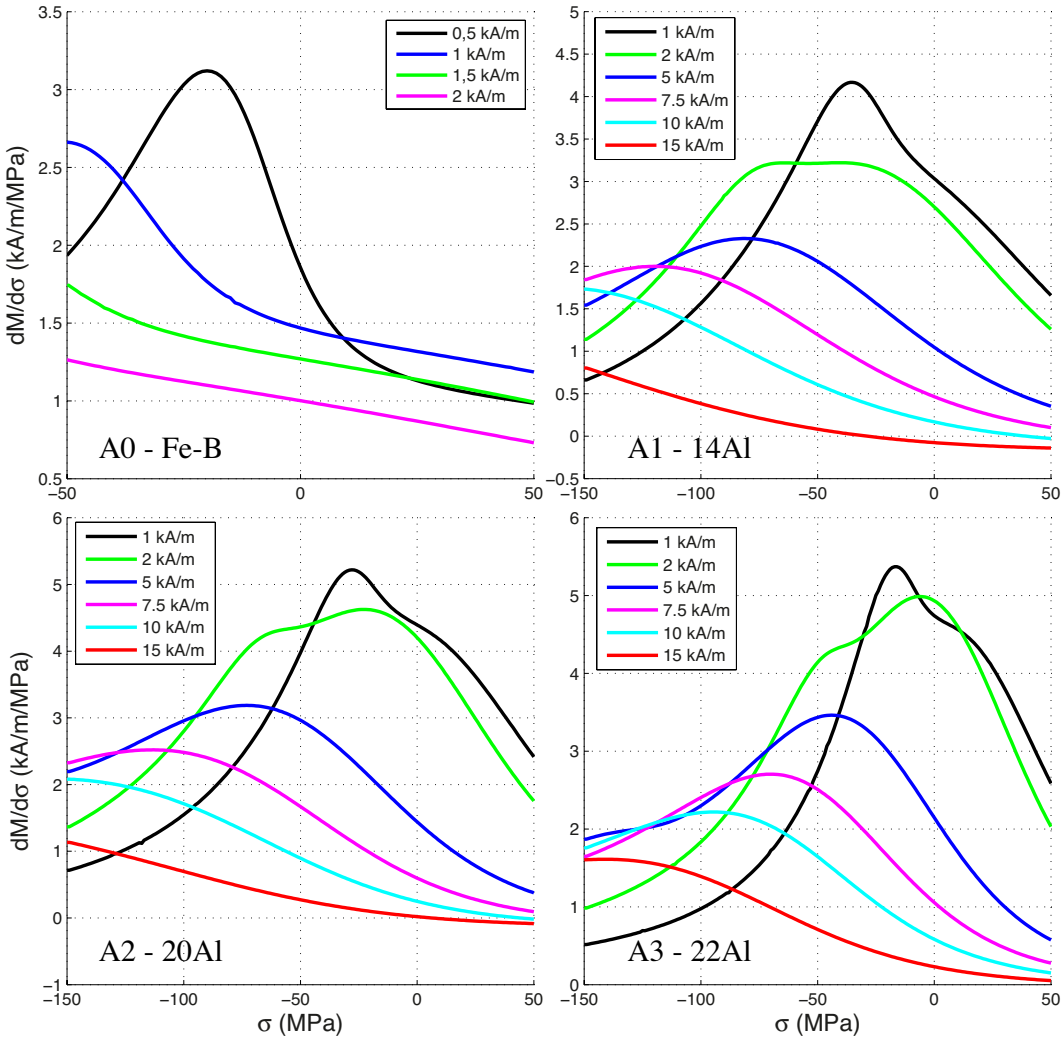

Figure 13: Modeling results: piezomagnetic sensitivity $dM/d\sigma|H$ *vs.* σ for all samples at fixed values of magnetic field, ($1 \leq H \leq 15$ kA/m).

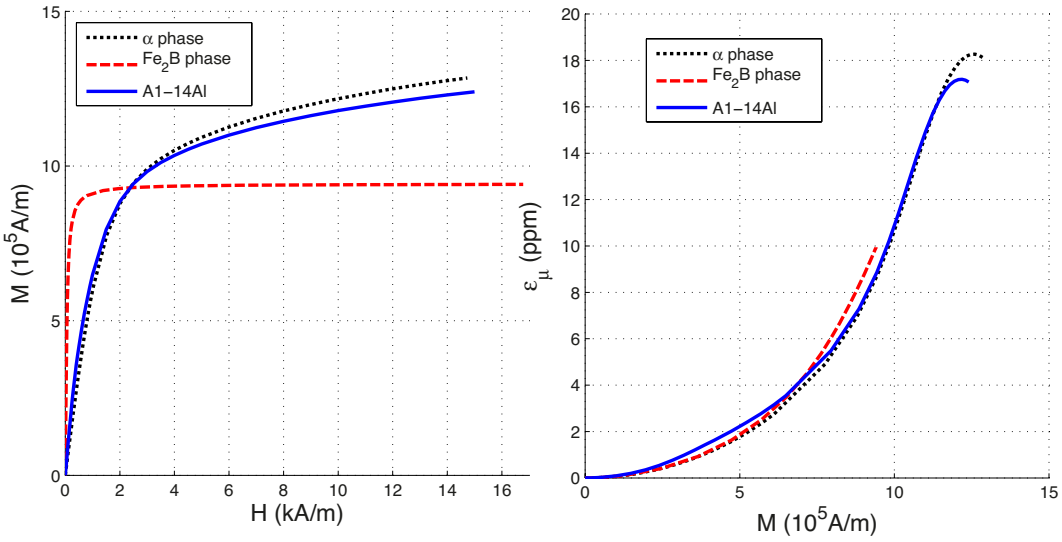

Figure 14: Modeled magnetic and magnetostrictive behaviors of both phases and average medium for $A1-14Al$ sample.

phenomenon explains the recent interest of scientific community for composite alloys. These figures show on the other hand, comparing to pure α phase, that improvement is strongly magnetic field dependent. Indeed, at 2kA/m magnetic field level, Fe_2B phase saturates. The pure α phase exhibits now a higher sensitivity than the composite. This effect combined with the reduction of susceptibility of α phase with increasing aluminum content explain the existence of an optimum combination of aluminum/boron content and magnetic field level.

Towards an optimization of piezomagnetic sensitivity

Improvement of piezomagnetic sensitivity is theoretically possible by choosing the appropriate aluminum/ boron content and texture for the material matrix. The model can help to reach this goal. Since sensitivity is related to variation of magnetostriction with field, the basic idea would be to choose the

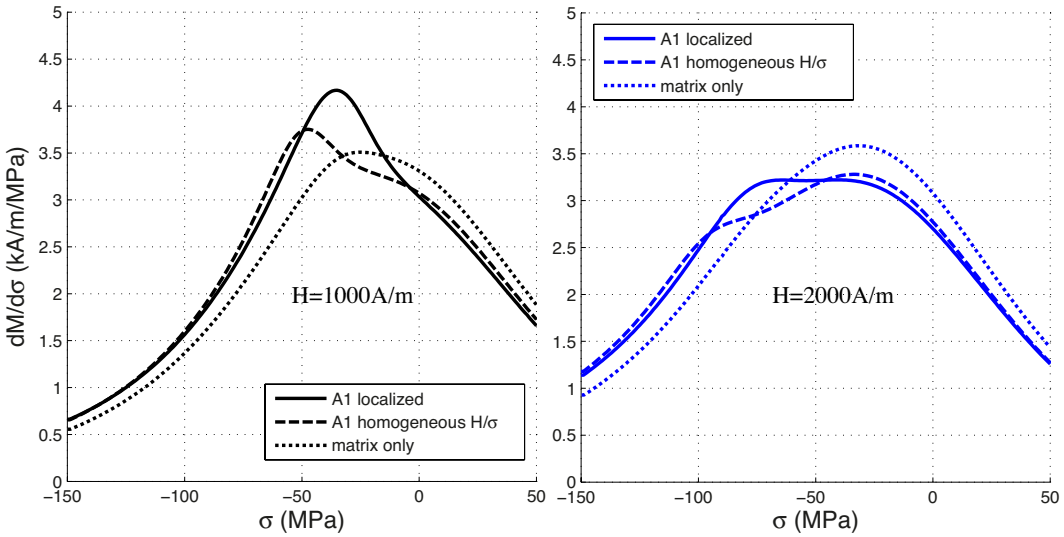

Figure 15: Modeled piezomagnetic sensitivity at two magnetic field level of: $A1-14Al$ α phase only, $A1-14Al$ sample considering localization, and $A1-14Al$ sample considering homogeneous stress and field.

composition leading to highest piezomagnetic effect and the crystallographic direction exhibiting the highest magnetostriction strain. By adjusting the field, it would be possible to create an improved Fe-Al-B alloys for sensor application. Alloy with 20%Al content is considered. Magnetostriction is high along the $< 100 >$ direction. We select this direction and model the piezomagnetic response in figure 16 for various magnetic field levels in a range of -100MPa to 50MPa. Maximal sensitivity level is about 15 kA/m/MPa. This value is 3 times higher than the value obtained for $A2-20Al$ sample exhibiting a less favorable orientation. Development of directional solidified samples seems relevant for a future application of these materials.

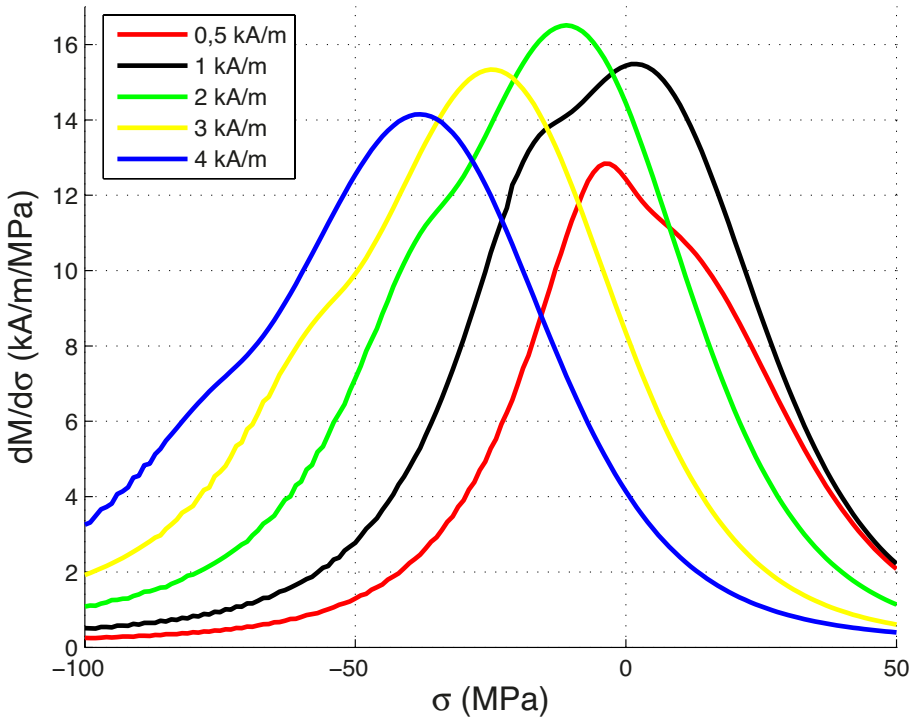

Figure 16: Modeled piezomagnetic sensitivity of ideal $<$ 100 $>$ oriented $(Fe - 20\%Al)_{98.4}B_{1.6}$ alloy at different magnetic field levels.

5. conclusion

Fe-Al-B alloy with 14% of aluminum and 1.6% of boron has a maximum sensitivity value for sensor performance of 4.0 kA.m^{-1}/MPa at -35 MPa for 2 kA/m. For the interval from 0 to -100 MPa the minimum sensitivity is about 1.5 kA.m^{-1}/MPa. Although the sensitivity is smaller compared to Terfenol D, the range of applied stresses is much higher and the applied field is much smaller [4]. The microstructure of Fe-Al alloys with low quantities of boron addition contains the Fe_2B phase. This phase does not degrade the sensing behavior of these materials, because Fe_2B has a high magnitude of the saturation magnetization [11]. Moreover, it enhances the sensing behavior due to both strong magnetic and mechanical localization effects by the increase of the initial susceptibility of the 14% of aluminum alloy at fields lower than 2.0 kA/m. Despite magnetostriction is strongly enhanced by an increase in aluminum content and magnetocrystalline anisotropy is lowered, the piezomagnetic behavior is not strongly improved. This can be explained by a lower permeability associated with enhanced magneto mechanical pinning effect. This effect is added to the fact that higher Al contents alloys have also low saturation magnetization magnitudes. An improvement of the piezomagnetic factor to 15 kA.m^{-1}/MPa is predicted, for the alloy with 20% of aluminum, by getting an adequate texture near $< 100 >$ directions. This would also favor the actuation behavior of the material. Discrepancies between experiments and modeling are due to many modeling approximations at different levels, representativeness of bulk texture from surface EBSD measurements, magnetostatic surface effects that are significant for high grain size materials. Moreover, for alloys with aluminum contents higher than 17% the existence

of ordering complicates the analyses. More studies are needed to better understand the effect of Fe_2B on the piezomagnetic behavior of these alloys.

6. acknowledgements

Financial supports from FAPESP under grant 2011/21258-0 and CAPES BEX under grant 10560/13-0 are gratefully acknowledged and also Prof. Hélcio J. Izário Fo. for the chemical analyses.

References

[1] D.C. Jiles, C.C.H. Lo, *Sensors and Actuators*, **A 106** (2003), pp. 3-7.

[2] C. Gourdin,L. Hirsinger, G. Barbier, R. Billardon, *Journal of Magnetism and Magnetic Materials*, **177-181** (1998), pp. 201-202.

[3] X.Bai, C.Jiang, *Journal of Rare Earths*, **28** (1) (2010), pp. 104-108.

[4] D. Kendall and A. R. Piercy, *Journal of Applied Physics*, **76** (1994), pp. 7148-7150.

[5] R. Grössinger, R. Turtelli, N. Mehmood, *IEEE Transactions on Magnetics*, **44** (11) (2008), pp. 3001-3004.

[6] R. C. Hall, *Journal of Applied Physics*, **30** (1959), pp. 816-819.

[7] N. Mehmood, R. SatoTurtelli, R. Grössinger, M. Kriegisch, *Journal of Magnetism and Magnetic Materials*, **322** (2010), pp. 1609-1612.

[8] L.-S. Hsu, G.Y. Guo, Y.-K. Wang, *Nuclear Instruments and Methods in Physics Research B*, **199** (2003), pp. 200-204.

[9] C.Bormio-Nunes, C.T. Santos, M. B. S. Dias, M. Doerr, S. Granovsky, M. Loewenhaupt, *Journal of Alloys and Compounds*, **539** (2012), pp. 226-232.

[10] C. Bormio-Nunes, M.B. Dias, L. Ghivelder, *Journal of Alloys and Compounds*, **574** (2013), pp. 467-471.

[11] W. Coene, F. Hakkens, R. Coehoorn, D.B. de Mooij, C. de Waard, J. Fidler and R. Grssinger, *Journal of Magnetism and Magnetic Materials*, **96** (1991), pp.189-196.

[12] A. Iga, Y. Tawara and A. Yanase, *J. Phys. Soc. Japan*, **21** (1966), 404.

[13] F. Mballa-Mballa, O.Hubert, S.Lazreg, P.Meilland, Multidomain modelling of the magneto-mechanical behaviour of dual-phase steels, proceedings of the 18th World Conference on Nondestructive Testing (WCNDT), 16-20 April 2012, Durban, South Africa.

[14] L. Daniel, O. Hubert, N. Buiron, R. Billardon. *Journal of the Mechanics and Physic of Solids*, **56** (2008), pp.1018-1042

[15] R. Hill, *Journal of the Mechanics and Physic of Solids*, **13** (1965), pp.89-101.

[16] O.Hubert, K.J.Rizzo, *Journal of Magnetism and Magnetic Materials*, **320** (2008), e979-e982.

[17] X. Wang, O. Hubert, S. He, F.S. Mballa-Mballa, Y. Huang, *Journal of Superconductivity and Novel Magnetism*, **27** (9) (2014), pp. 2049-2058.

[18] S. Lazreg, O. Hubert, *Journal of Applied Physics*, **9**, 07E508 (2011).

[19] J. M. Cook and S. Pavlovic, *Journal of Applied Physics*, **50** (1979), pp. 7710-7712.

[20] E. Du Trémolet de Lacheisserie, D.Gignoux, M.Schlenker, Magnetism-I, *Springer Science & Business Media*, 2005.

[21] L. Daniel, N. Galopin, *European Physical Journal - Applied Physics*, **42** (2008), pp.153-159.

Appendix A. Magnetic and magnetostrictive behavior of Fe_2B phase

The Fe_2B phase is a tetragonal phase with $CuAl_2$ (C-16) prototype structure. Even if it is not a well known material, it is possible to find some partial informations about its physical constants, magnetic and magnetostrictive behavior in references [9, 11, 12] It is a ferromagnetic material with $T_C^{Fe_2B} =$ 742°C. The anisotropy constant (uniaxial anisotropy) is high reaching K_1=-4.27 $\times 10^5$ J.m^{-3} at room temperature and goes to zero at 251°C [12]. Due to uniaxial anisotropy Fe_2B exhibits an easy (001) plane. The magnetization behavior of isotropic polycrystalline Fe_2B is reported in figure A.17a exhibiting a saturation magnetization of 1.2×10^6 A/m [11]. The magnetostrictive behavior of isotropic polycrystalline Fe_2B is reported in figure A.17b [9] (the demagnetizing field due to form effect - cubic sample - has not been removed explaining the high magnetic field level required to create a significant magnetostriction strain). The saturation magnetostriction is estimated to be 20 ppm. The magnetostriction is supposed isotropic at the grain scale in the paper. It is a strong hypothesis than cannot be verified.

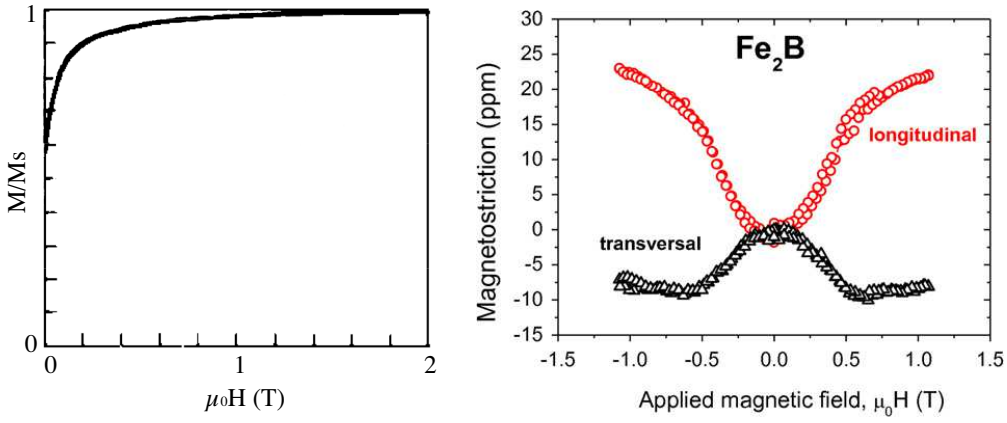

(a) (b)

Figure A.17: (a) Magnetization curve of Fe_2B as reported in [11]; Magnetostriction behavior of Fe_2B as reported in [9].

Coene *et al.* [11] reported in figure A.17a a very sharp increase of M at low field. This can be understood by a simple magnetization rotation model in the easy plane.

Appendix A.1. Theoretical estimation of magnetization behavior

An isotropic distribution of Fe_2B grains is considered. This means that quadratic $\vec{c}-$axis is regularly distributed in a unit radius sphere. $\vec{c}-$axis is given using spherical parameters α_1 and β by:

$$\vec{c} = \begin{pmatrix} cos\alpha_1 \\ cos\beta sin\alpha_1 \\ sin\beta sin\alpha_1 \end{pmatrix} \tag{A.1}$$

The magnetization vectors are for the same reason regularly distributed inside the easy plane of particles. This point is illustrated in figure A.18a: the

average magnetization is null.

The in-plane magneto-crystalline anisotropy is probably very low in accordance with experimental data. A weak magnetic field H applied in direction $\vec{x}$ is consequently enough to select the most favorable direction in the easy plane with respect to the magnetic field direction. The selected vector is denoted $\vec{u}$. It belongs to the ($\vec{c}-$axis, $\vec{x}$) plane so that:

$$\vec{u} = \begin{pmatrix} cos(\pi/2 - \alpha_1) \\ -cos\beta sin(\pi/2 - \alpha_1) \\ sin\beta sin(\pi/2 - \alpha_1) \end{pmatrix} = \begin{pmatrix} sin\alpha_1 \\ -cos\beta cos\alpha_1 \\ -sin\beta cos\alpha_1 \end{pmatrix} \tag{A.2}$$

This point is illustrated in figure A.18b. At the saturation $\vec{u}$ rotates progressively in direction to $\vec{x}$. The average magnetization is the saturation magnetization.

For all conditions, calculating an average $\vec{u}$ direction denoted $< \vec{u} >$ leads to calculate the associated magnetization supposing that each $\vec{u}$ defines one magnetization direction.

- without magnetic field, it is obvious that the average magnetization is null.

- under a moderate magnetic field, average $< \vec{u} >$ direction can be calculated following:

$$< \vec{u} >= \frac{1}{2\pi} \int_0^{2\pi} \int_0^{\pi/2} \vec{u}\, sin\alpha_1\, d\alpha_1 d\beta = \frac{1}{2\pi} \int_0^{2\pi} \int_0^{\pi/2} sin^2\alpha_1\, d\alpha_1 d\beta\, \vec{x} \tag{A.3}$$

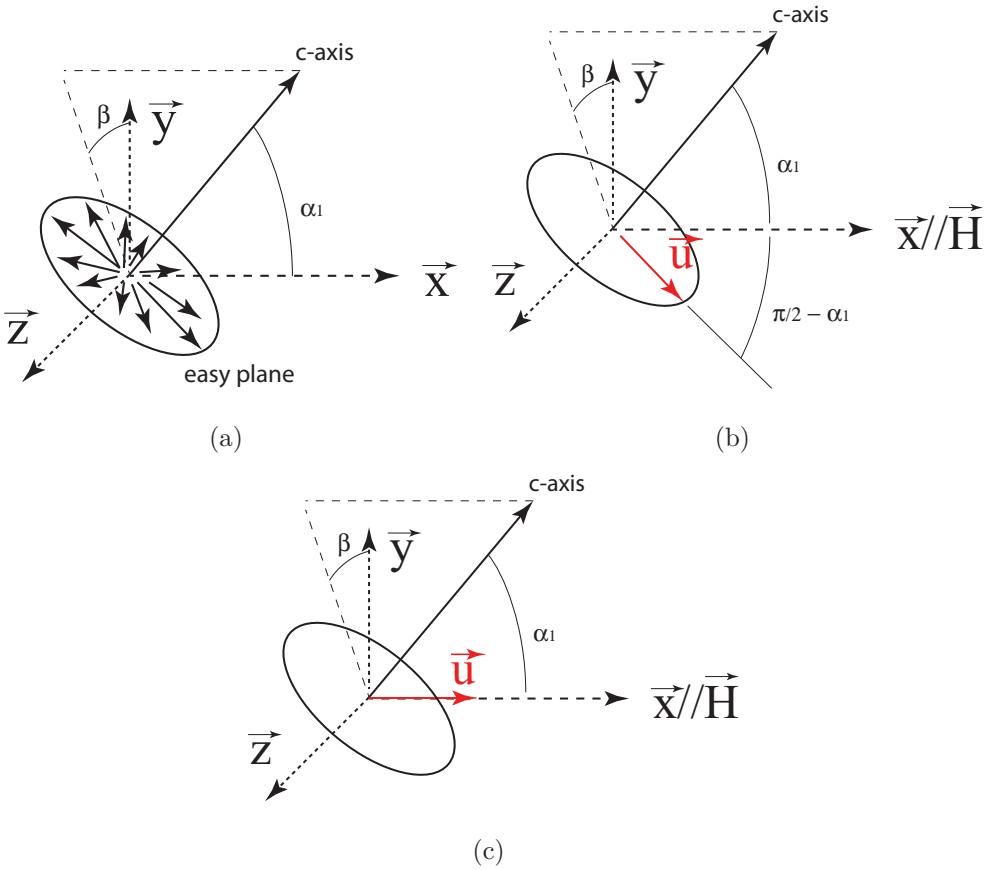

Figure A.18: Illustration of magnetization distribution at different magnetization levels: (a) without magnetic field, multiple directions are regularly distributed inside the easy plane; (b) under low magnetic field, one unique direction inside easy plane is selected before rotation; (c) high magnetic field leads to a magnetization rotation.

we obtain:

$$< \vec{u} >= \pi/4\,\vec{x} \tag{A.4}$$

The magnetization is given by:

$$\frac{M}{M_s} = \frac{\pi}{4} \approx 0.785 \tag{A.5}$$

568 This result is in accordance with the results of Coene *et al.* [11].

- at saturation, the following result is obviously

$$< \vec{u} >= \vec{u} = \vec{x} \qquad \text{and} \qquad \frac{M}{M_s} = 1 \tag{A.6}$$

This magnetization can be achieved with a field high enough to overcome the uniaxial anisotropy (about 2T following Coene's results [11])

Appendix A.2. Theoretical estimation of magnetostriction

A theoretical estimation of magnetostriction is possible following the procedure used for the magnetization, using the descriptions in figure A.18. At zero applied field, the magnetization vectors are regularly distributed inside the easy plane of particles, the average magnetostriction is null. As discussed above, a weak magnetic field H applied in direction $\vec{x}$ is enough to select the most favorable direction in the plane with respect to the magnetic field direction. The selected vector is $\vec{u}$ given by equation (A.3). The components of $\vec{u}$ are the direction cosines γ_i of the magnetization. They are used in the definition of the magnetostriction tensor for isotropic conditions (as supposed for Fe_2B):

$$\boldsymbol{\epsilon}_{\mu}^{\vec{u}} = \frac{3}{2}\lambda_s \begin{pmatrix} (\gamma_1^2 - \frac{1}{3}) & \gamma_1\gamma_2 & \gamma_1\gamma_3 \\ \gamma_1\gamma_2 & (\gamma_2^2 - \frac{1}{3}) & \gamma_2\gamma_3 \\ \gamma_1\gamma_3 & \gamma_2\gamma_3 & (\gamma_3^2 - \frac{1}{3}) \end{pmatrix} \tag{A.7}$$

An average magnetostriction tensor is calculated now so that:

$$< \boldsymbol{\epsilon}_{\mu}^{\vec{u}} >= \frac{1}{2\pi} \int_0^{2\pi} \int_0^{\pi/2} \boldsymbol{\epsilon}_{\mu}^{\vec{u}} \, sin\alpha_1 \, d\alpha_1 d\beta \tag{A.8}$$

After few calculations the following result is obtained:

$$< \boldsymbol{\epsilon}_{\mu}^{\vec{u}} >= \begin{pmatrix} \frac{\lambda_s}{2} & 0 & 0 \\ 0 & -\frac{\lambda_s}{4} & 0 \\ 0 & 0 & -\frac{\lambda_s}{4} \end{pmatrix} \tag{A.9}$$

so that the longitudinal magnetostriction reaches $\lambda_s/2$ at very low field for a magnetization of about 0.785 M_s.

At the saturation, $\vec{u}$ rotates progressively in direction to $\vec{x}$. The average magnetostriction is the saturation magnetostriction λ_s itself. This is reached for a very high magnetic field level.

Appendix A.3. Consequence in term of modeling for present paper

The magnetic field level used in the experiments presented in the paper is not enough to begin the rotation mechanism. For simplicity reasons, the in easy plane rotation mechanism has only been considered for the modeling of magnetic and magnetostrictive behaviors of the Fe_2B phase (see section 4.3). Fe_2B phase has been considered as an isotropic very soft phase (K_1=0; χ_0=8000) with apparent saturation magnetization $M_s^{'Fe_2B}=(\pi/4)M_s^{Fe_2B}=9\times 10^{-5}$A.m^{-1} and apparent saturation magnetostriction $\lambda_s^{'Fe_2B} = \frac{1}{2}\lambda_s^{Fe_2B}$=10 ppm. Figures A.19a and A.19b show the obtained modeled magnetization and magnetostrictive behaviors in the magnetic field range of the work presented in the paper. These modeling are in accordance the few available experimental data for this material.

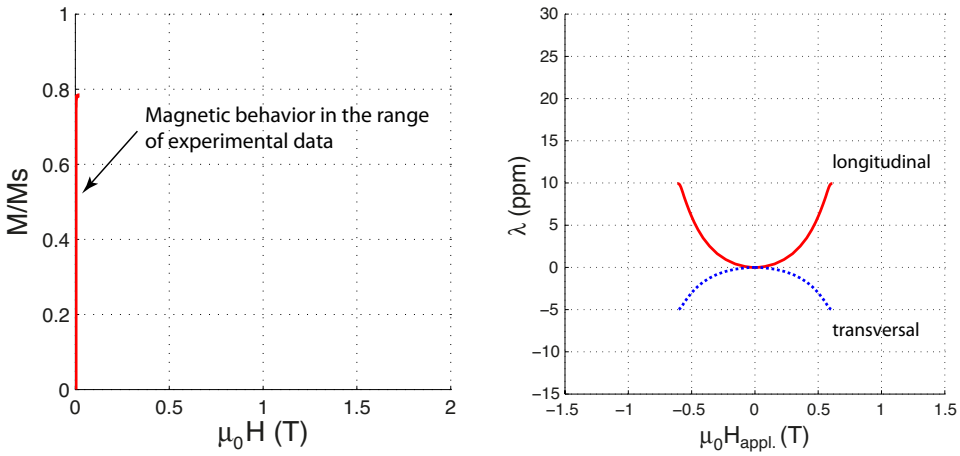

(a) (b)

Figure A.19: Modeled magnetization and magnetostrictive behavior of Fe_2B phase in the magnetic field range of the work presented in the paper - to be compared to experimental results reported in figures A.17a and A.17b (a cubic form effect is considered to define the applied magnetic field in figure (b).